Volume 17
Number 1
7 January 2026
Pages 1–674

Chemical Science

rsc.li/chemical-science

ISSN 2041-6539

ROYAL SOCIETY OF CHEMISTRY

EDGE ARTICLE

Chong Fang *et al.*

Ultrafast spectroscopic signatures for *off*-to-*on* photoswitchable species in a green-to-red photoconvertible fluorescent protein

Chemical Science

ROYAL SOCIETY OF CHEMISTRY

EDGE ARTICLE

View Article Online
View Journal | View Issue

Cite this: *Chem. Sci.*, 2026, **17**, 151

All publication charges for this article have been paid for by the Royal Society of Chemistry

Ultrafast spectroscopic signatures for *off*-to-*on* photoswitchable species in a green-to-red photoconvertible fluorescent protein

Taylor D. Krueger, Cheng Chen and Chong Fang *

Photoconvertible fluorescent proteins (pcFPs) have greatly advanced life sciences and cellular imaging with sub-diffraction resolution. A subset of Kaede-like pcFPs can reversibly photoswitch and irreversibly photoconvert, which yield intriguing properties for sophisticated bioimaging, yet blinking may complicate image analysis. Many investigations on such pcFPs lack transient information that can dictate their optical properties, especially on ultrafast timescales. We study a family of ancestrally derived pcFPs with varying photoconversion and photoswitching efficiencies based on the least evolved ancestor (LEA). With ultrafast electronic and vibrational spectroscopies that complement steady-state measurements, we dissect the primary events upon near-UV excitation of the native and photoswitched neutral chromophores, which initiates both *off* → *on* photoswitching and green-to-red photoconversion. We demonstrate that *cis* → *trans* isomerization underlying negative photoswitching occurs the fastest in acidic buffers upon green light irradiation, which forms a distorted neutral *off* state proportional to the initial green *cis* anionic population. Femtosecond transient absorption measurements reveal that this dynamic *off* state rapidly photoswitches back to the bright on state upon near-UV excitation, in contrast to the native form. With various mutants and photoinduced states, we find that *off* → *on* photoswitching likely involves excited state proton transfer from the distorted chromophore, which competes with photoconversion. In contrast, femtosecond stimulated Raman spectroscopy (FSRS) of the much less photoswitchable LEA-A69T tracks the efficient nonradiative relaxation of the native *cis* neutral chromophore. We propose rational design strategies to inhibit *off* → *on* photoswitching while improving the photoconversion efficiency of both neutral states. This work is envisioned to inspire more dynamic investigations of diverse photochromic FPs on ultrafast timescales.

Received 18th August 2025
Accepted 29th November 2025

DOI: 10.1039/d5sc06279a

rsc.li/chemical-science

Introduction

Photoconvertible fluorescent proteins (pcFPs) are instrumental bioprobes for advanced imaging techniques.[1,2] The Kaede-like green-to-red pcFPs bearing the three-residue His-Tyr-Gly chromophore are particularly useful for bioimaging techniques like photoactivated localization microscopy (PALM).[3] Certain aspects of the green-to-red photoconversion mechanism are well understood, including the ubiquitous peptide cleavage occurring alongside the chromophore conjugation extension that effectively redshifts the biomolecular optical spectra.[4] However, due to the low photoconversion quantum yield and broad timescales proposed ranging from femtoseconds (fs) to milliseconds, pertinent key details regarding the photoconversion mechanism remain elusive. While there have been important modifications to Kaede-like pcFPs for improving performance, unknown mechanistic aspects hinder the rational design of more advanced bioprobes with targeted optical properties.

Many of these fascinating proteins are based on the same motif and feature similarities in terms of interactions between the chromophore and local environment; however, even the mutation of one residue can have drastic influences on the static and dynamic optical properties of the chromophore. Several Kaede-like pcFPs including IrisFP,[5,6] mEos,[7] pcDronpa,[8] Dendra,[9] LEA,[10–12] and more possess the unique ability to repeatedly photoswitch following light activation at certain wavelengths in addition to irreversible photoconversion. The photoswitched dark "*off*" state typically consists of a *trans* or *trans*-like distorted structure[13] that forms upon negative photoswitching *via cis* → *trans* isomerization by illuminating the bright *cis* anionic "*on*" state with green light (Fig. 1). In this subcategory of pcFPs, the "*off*" state (GA′) corresponds to the neutral protonated chromophore and remains in a metastable state at thermal energy for hours-to-days before eventually relaxing to the bright *cis* resting state (GB).[14,15] However, the photoswitched "*off*" state efficiently returns to this resting state upon gentle irradiation with ~400 nm light, typically with

Department of Chemistry, Oregon State University, 153 Gilbert Hall, Corvallis, Oregon 97331, USA. E-mail: Chong.Fang@oregonstate.edu; Web: https://fanglab.oregonstate.edu/

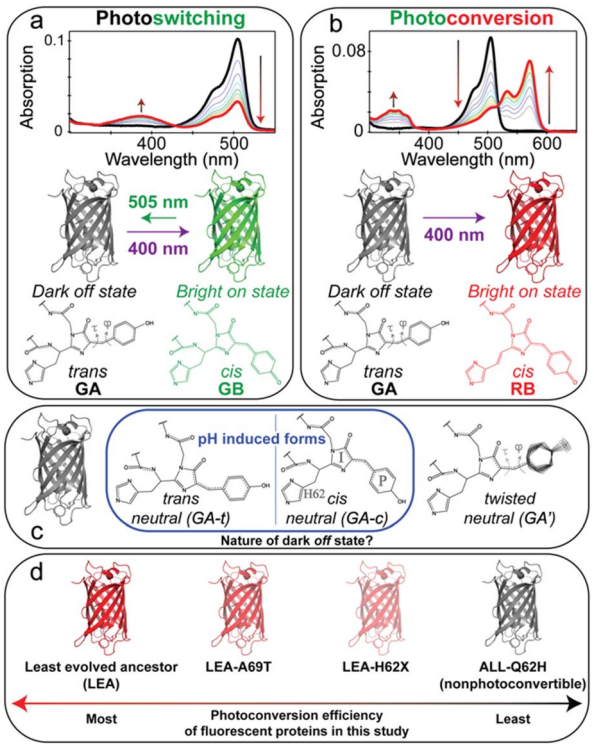

Fig. 1 Illustration of (a) photoswitching and (b) photoconversion in LEA proteins. (c) Proposed chromophore conformations in the "dark" neutral state of LEA. The P-, I-, and far imidazole (H62) rings are labelled. (d) Photoconversion efficiencies of fluorescent proteins in this work.

a much higher quantum yield than the *on* → *off* photoswitching. This unique ability to photoswitch and photoconvert adds to the complexity toward understanding the photodynamic behaviour of these biomolecules; for example, molecular blinking can complicate image analysis and lead to overcounting in super- resolution imaging.[16] However, this photochromic behaviour also leads to additional layers of external control of bright or dark states that can be exploited during sophisticated imaging techniques including the monitoring of dynamic processes.

While the engineered least evolved ancestor (LEA) displays unexpected photoswitching,[14] it was originally designed as a scaffold to understand how photoconversion may have evolved from the ancestral green fluorescent protein (ALL-GFP). The LEA protein bears the minimal number of mutations to enable efficient photoconversion from the non-photoconvertible ALL-GFP, which was modified to produce ALL-Q62H by a single-site substitution that incorporates a histidine residue into the chromophore structure. The Kaede-like chromophore in ALL-Q62H remains non-photoconvertible, highlighting the dynamic chromophore–environment interactions as important factors for photoconversion and optical properties of the protein.[17] Two other mutants feature key single-site mutations from LEA (LEA-A69T and LEA-H62X), which display varying degrees of photoswitching and photoconversion capabilities (Fig. 1d).[18,19]

Given the consensus that photoconversion starts from the neutral (protonated) green chromophore (GA), there remains debate whether GA is *cis* or *trans*. Since the efficient *off* → *on* photoswitching and the rather inefficient photoconversion are both triggered by near-UV (~400 nm) irradiation of GA/GA′, does photoswitching actively compete with photoconversion or produce an intermediate toward the photoconverted product? To tackle this question, we exploit a set of recently engineered LEA derivatives displaying various photochromic efficiencies to enable a systematic evaluation of photophysical properties *via* steady-state and ultrafast electronic/vibrational techniques. The largely unchanged chromophore–environment interactions before/after photoconversion suggest that transient dynamics play a key role,[19–21] highlighting the importance of such ultrafast measurements to dissect reaction intermediates inside FPs.

Notably, we performed steady-state optical spectroscopy involving sequential light irradiation on LEA under various buffer pH conditions to better distinguish the photophysical properties of the chemically equilibrated GA and photoinduced GA′ species. We previously showed that GA′ can photoconvert, albeit less efficiently than GA,[14] so we aim to shed new light on the photoconversion mechanism by comparing the primary events in contrasting FPs after near-UV excitation with femtosecond transient absorption (fs-TA) spectroscopy. The photoswitched *off* state (GA′) and mutants with reduced photoconversion efficiencies display a pronounced biphasic rise of the stimulated emission feature assigned to the *cis* anionic chromophore (GB), which is absent in the pH-induced (GA) population in LEA. This result suggests that *off* → *on* photoswitching may compete with and quench the photoconversion. Femtosecond stimulated Raman spectroscopy (FSRS)[22–25] provides structural information on the neutral chromophore population, tracking excited-state GA* vibrational signatures that rapidly decay on the femtosecond-to-picosecond (fs-to-ps) timescale for efficient nonradiative relaxation of the flexible chromophore. The LEA chromophore structure and local environment are compared with several other photochromic Kaede-like pcFPs to inspire future ultrafast investigations of these versatile and functional biomolecules, thereby providing more rational and targeted design principles for efficient protein and bioprobe/biosensor engineering.

Results and discussion

pH-dependent GA′ formation in the LEA *via on*-to-*off* photoswitching

Relative to other Kaede-like pcFPs, the elevated pK_a of LEA (6.3) allows for an in-depth comparison of GA and the metastable GA′ chromophores in aqueous buffers with physiologically relevant pH values. The photoconversion efficiency has been studied under several buffer pH conditions, and it has been observed that the optimal photoconversion occurs at pH 6.1;[11] however, the recently discovered photoswitching behaviour in LEA has not been investigated as a function of pH. We studied LEA under 505 nm irradiation in buffer solutions with pH values from 6 to 8 (Fig. 2) to investigate how the charge/protonation states of the FP local environment residues (*i.e.*, protein

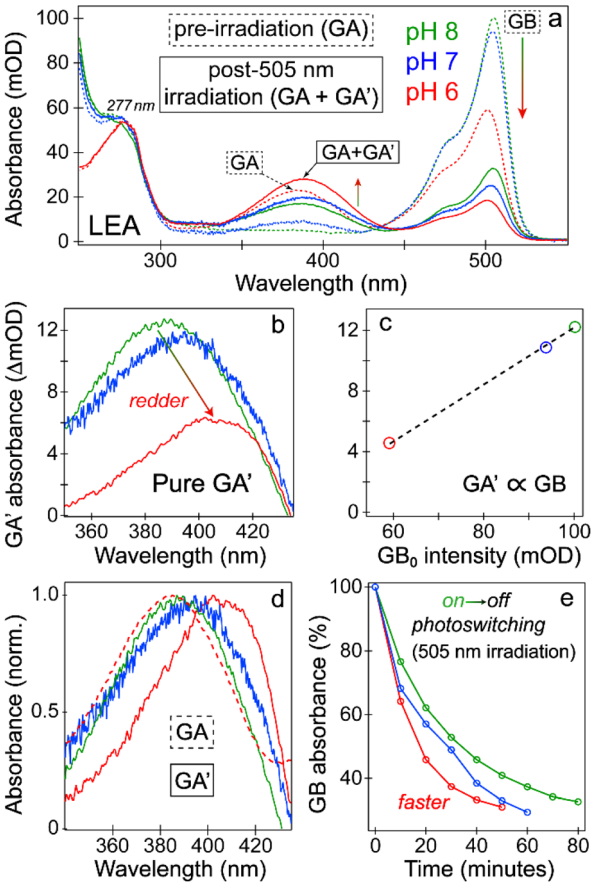

Fig. 2 The pH-dependent steady-state absorption spectra of LEA under 505 nm illumination. (a) UV/vis absorption spectra of LEA before (dashed) and after (solid) 505 nm illumination in pH 8 (green), 7 (blue), and 6 (red) buffers. The spectra, scaled to 277 nm, represent an equal total FP concentration regardless of the buffer pH. (b) Pure GA′ absorption spectra produced after 505 nm illumination by taking the difference, (GA + GA′) − GA, from panel a. (c) Plot of GA′ absorption intensity against the initial GB intensity (GB_0) before 505 nm irradiation. The circle size represents the largest (at pH 7) spectral data deviation (at 1 s.d.) from the center value, which reflects the uncertainty of measurements. (d) The normalized absorption spectra of GA′ (solid color-coded) in each buffer *versus* GA in pH 6 buffer (dashed red). (e) Decay of GB absorption intensity (%) as a function of time during *on* → *off* photoswitching under 505 nm illumination (color-coded, three pH conditions). The absorption intensities in (a–c) are in milli-optical-density (mOD) units.

matrix) may affect the *on* → *off* photoswitching and the optical properties of the GA′ *versus* GA species.

As expected from the chromophore pK_a, fresh proteins that have not been exposed to light irradiation display a progressive reduction of the *cis* anionic form (GB) absorption peak at ~505 nm and a concurrent rise of the protonated form absorption band at ~380 nm (GA) as the buffer pH decreases (Fig. 2a). A slight blueshift of the GB peak is observed in the more acidic buffer, indicating that local-environment residues with certain modified charge or protonation states can affect the spectroscopic properties of the chromophore. After 505 nm light irradiation of the fresh LEA protein sample, a large decrease in the GB absorption band is matched by a moderate increase in the neutral absorption band assigned to GA′ formation, reflecting the greatly reduced transition oscillator strength of the *trans* neutral *versus* the *cis* anionic chromophore. An analysis of the relative absorption peak intensities of GA, GA′, and GB revealed that the oscillator strength of GA′ is reduced by ~60–70% relative to GA (see Table S1 in the SI), indicative of a distorted chromophore that has been proposed in Kaede-like pcFPs.[14,26] The metastability of GA′ that slowly recovers over days in the dark suggests that chromophore interactions with the protein local environment can stabilize the GA′ population and raise the reaction barrier height to hinder the *off* → *on* thermal recovery. Moreover, the redshifted GA′ absorption peak following 505 nm irradiation *versus* that of GA without any irradiation (Fig. 2a and d) supports a distorted conformation of GA′.

Taking the difference between (GA + GA′) and GA spectra, we obtained a pure GA′ absorption band in each pH environment (Fig. 2b), revealing a distinct redshift of the GA′ band as the buffer pH decreases. This result shows that GA′, unlike GA, is especially sensitive to the charge/protonation states of the local environment (*e.g.*, an adjacent His194 likely becomes protonated when pH drops from 8 to 6, see below). Notably, the GA′ absorption peak drops at a lower pH. In fact, plotting the initial GB absorption intensity before any irradiation (GB_0) in three pH conditions against the final GA′ intensity after 505 nm irradiation reveals a linear trend (Fig. 2c): the amount of GA′ formed is proportional to the initial GB population (also see Fig. S1, SI). Therefore, the *cis* → *trans* isomerization model[27] holds for LEA's *on* → *off* photoswitching under 505 nm illumination, as also indicated by the isosbestic point supporting a two-state model (Fig. 2a).

It has been hypothesized that the pK_a of GA′ is higher than that of GA, primarily because the neutral form population increases after *on* → *off* photoswitching while the buffer pH remains the same.[15,18] Since we observed that the amount of GA′ formed in LEA is largely insensitive to pH values of 6–8, the pK_a of GA′ is well above 8, corroborated by the *trans* chromophore in Kaede-like pcFPs with a pK_a > 10.[2] Due to intrinsic heterogeneity in the protein matrix, there may be some *cis*-distorted GA′ populations in more acidic buffers (Figs. 1c, 2d) as shown by the redshifted but still broad absorption at pH 6, proposed in photoswitchable pcFPs like mEos4b[15,28] and reversibly switchable fluorescent proteins (rsFPs).[29] The pK_a of *cis*-GA in LEA[11] was determined to be 6.3, so the pK_a of *cis*-GA′ is likely above 6.3, leading to more *cis*-GA′ population as the buffer pH decreases.

Such a conformational heterogeneity can be rationalized by chromophore–environment interactions, particularly for the neutral chromophore having fewer electrostatic interactions with the local environment, thus promoting flexibility *versus* the anionic chromophore. Some *trans*-neutral to *cis*-neutral equilibration may occur, in accord with the aforementioned frustrated GA′ conformation inside an irradiated protein matrix, supported by some *off* → *on* thermal recovery that we observed under the dark-adapt condition (*i.e.*, without light exposure).[18] Future investigations using advanced structural techniques[30–32] should provide new insights into such interconversion events. For more evidence, we calculated the electronic absorption

spectra of the *cis* and *trans* neutral green chromophore *in vacuo* and predicted that the *trans* conformer absorbs redder than the *cis* conformer (Fig. S2, SI),[33] corroborating the continuous redshift of the GA′ absorption peak with a significantly smaller oscillator strength than that of GA (Fig. 2b). Future experimental and computational studies factoring interactions between *trans*/*cis* neutral species and their local environment will be required to investigate the steady-state and dynamic heterogeneity more rigorously.[15,18,28] For instance, primary events may differ upon excitation of *trans*, *cis*, or distorted neutral species to critically affect the FP photoswitching and photoconversion efficiencies. Furthermore, the mechanistic implications for photoconversion due to the currently unclear starting conformation(s) are set to provide profound insights into photoconversion.[27,34]

Notably, the *on* → *off* photoswitching accelerates in more acidic buffers (Fig. 2e). The time-dependent contour plots (Fig. S3, SI) manifest spectral evolution on the minute timescale under 505 nm irradiation and the redshifted GA′ formation in pH 6 buffer. By plotting the GB and GA′ absorption intensities as a function of time (Fig. S4, SI), we estimated the *on* → *off* photoswitching rate constant in each buffer pH. The increased *on* → *off* photoswitching efficiency in more acidic buffers also correlates with the photoconversion efficiency,[11] highlighted for LEA in pH 6 *versus* 8 buffers under 400 nm illumination (Fig. S5, SI). This finding implies that acidic pH values induce changes in the protonation states of the surrounding residues and provide a more flexible chromophore environment, which supports prior molecular dynamics simulations suggesting that chromophore structural dynamics are important for photoconversion.[17]

Off-to-*on* photoswitching of GA′ in LEA upon 400 nm excitation forms GB′

We measured fluorescence with UV (360–400 nm) excitation across buffer pH values of 6–8 to investigate the interplay between *off* → *on* photoswitching and GA/GA′ photoconversion (Fig. 3). We focus on the emission spectra in pH 8 buffer after 400 nm excitation because this wavelength has been commonly used in bioimaging, while it allows a straightforward connection to the fs-TA measurements (see below). This buffer represents a physiologically relevant pH and a more direct evaluation of GA′, since at pH 8 there is minimal GA to begin with. Steady-state emission spectra with other excitation wavelengths and buffers can be found in the SI (Fig. S6) for detailed comparisons.

The emission spectra of GA and (GA + GA′) reveal that both species are weakly fluorescent (Fig. 3a). The photoinduced *off* state exhibits increased emission from ~420–480 nm, where the neutral form emits, in part because the absorption intensity at the excitation wavelength is elevated due to GA′ (Fig. 3b). We isolated the GA emission (Fig. S7, SI) without spectral overlap from GB emission above ~470 nm. The most striking aspect after GA excitation is the dominant emission from the anionic green chromophore (GB), which may occur *via* several pathways (see below) and is intrinsic to the chromophore featuring a much larger oscillator strength of GB than GA.[11,24,35] The

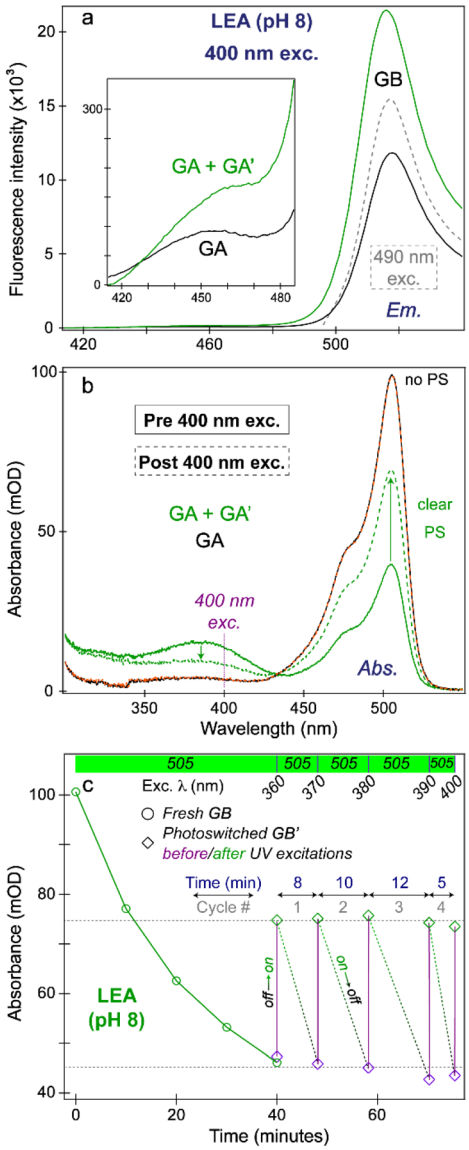

Fig. 3 Steady-state (a) emission and (b) absorption spectra of GA + GA′ (green) and GA (black) in pH 8 buffer. The emission spectra upon 400 nm excitation are overlaid with the GB emission spectrum upon direct (490 nm) excitation (grey dashed). Weak emission of the neutral chromophore from ~420–480 nm is shown in the inset. In panel b, solid/dashed traces represent the electronic absorption spectra before/after the fluorescence measurements in panel a with 400 nm excitation. Green arrows indicate the major spectral changes upon excitation of GA + GA′. The dashed orange trace shows that there is no major absorption change after 400 nm excitation of GA. (c) Absorption intensities of fresh GB (circles) and GB′ (diamonds) before/after (purple/green) 360–400 nm (UV) excitations. Horizontal green bars represent the time duration of 505 nm illumination on LEA. The photocycle number and time (minutes) under 505 nm illumination of GB′ to regenerate GA′ are listed for each photocycle.

broad, weak emission of GA and GA′ (inset of Fig. 3a) supports flexibility of a *trans* neutral chromophore with more heterogeneity in the excited state and enhanced nonradiative relaxation.[15,33] There is no clear trend for emission peak wavelengths or band shapes of GA/GA′ from pH 6–8 with 360–400 nm excitation (Fig. S6, SI), suggesting that the local environment exerts

a minor effect on the fluorescent state, unlike the absorption from the electronic ground state (S_0). While the broad spectral profiles suggest heterogeneity, there is no evidence for distinct subpopulations. Moreover, there is no clear signature of GA′ emitting species, although the emission profile appears slightly redshifted from that of GA which is similar to the trend for absorption bands (Fig. 2).

One property change becomes apparent upon (near)-UV excitation of GA *versus* GA. GA′ is significantly more prone to *off* → *on* photoswitching. This is demonstrated by the changed absorption spectra before/after UV-excitation (Fig. 3b), which manifests more/less of GB/GA′ after light activation. The rapid *off* → *on* photoswitching supports the notion that GA′ features a distorted conformation and frustrated interactions with the local environment. In contrast, the absorption spectra before/after excitation of GA do not change (Fig. 3b), indicating that GA does not undergo *off* → *on* photoswitching which is supported by steady-state measurements with a larger GA population in more acidic buffers (Fig. S6, SI). In general, upon excitation of GA/GA′, there are primarily three pathways through which GB emission can occur: (1) direct excitation of GB, (2) Förster resonance energy transfer (FRET),[36–38] and (3) excited state proton transfer (ESPT).[21,22,35,39] Direct GB excitation is unlikely given the large energy difference between the excitation wavelength and GB absorption peak. Indeed, the GB emission intensity upon excitation of (GA + GA′) is about twice more intense than that in the GA excitation case (Fig. 3a), refuting direct excitation playing a large role because the GB absorption (Fig. 3b, black trace) is much stronger than that after 505 nm illumination in order to generate GA′ (Fig. 3b, green trace).

Meanwhile, FRET could occur because LEA is a tetrameric pcFP like other Kaede-like pcFPs,[5,11] and the chromophore–chromophore distances among four subunits are a function of geometry. FRET was proposed for Kaede-like FPs with similar tetrameric geometries to LEA.[40–42] Subsequent analysis of the steady-state absorption/emission spectra (Fig. S8, SI) and fs-TA measurements suggest that FRET may contribute; however, neither FRET nor direct excitation can cause the equilibrium change before and after UV excitation of GA′ as evidenced by the absorption spectra (Fig. 3b). We confirmed this change during the fluorescence measurements by varying the slit width as well as scan speed (Fig. S9, SI). Given that excitation of the neutral species leads to emission from the anionic form, proton transfer likely occurs in the electronic excited state or ground state, reported to generally occur in FPs[22,43] and Kaede-like pcFPs,[42] motivating a series of fs-TA measurements (see below).

Interestingly, after at least one photocycle (*on* → *off* under 505 nm illumination and then *off* → *on* under 360–400 nm excitation), we observed that GA′ was likely converted to a new form of the anionic green chromophore (GB′), reminiscent of the previously reported *cis* anionic chromophore under 400 nm illumination of the fresh LEA at pH 7.9, wherein calculations pointed to a distorted chromophore with a twisted phenolate ring.[14] Recently, other reports identified the photoinduced heterogeneity of green as well as red *cis* chromophores in Kaede-like pcFPs.[15,28] The new evidence for GB′ in the LEA is provided by the much faster *on* → *off* photoswitching after one photocycle (Fig. 3c). An example of the absorption spectra before/after 400 nm excitation is shown (Fig. 3b), corresponding to GB′ absorption intensities (Fig. 3c). The *off* → *on* photoswitching occurs rapidly (4–5 seconds) upon 360–400 nm excitation, whereas the *on* → *off* photoswitching proceeds on the minute timescale, in accord with the much larger *off* → *on* photoswitching quantum yield (psQY) than the *on* → *off* psQY commonly observed for photoswitchable Kaede-like pcFPs and other rsFPs.[44] The absorption and emission spectra are shown in all three buffers (Fig. S10, SI), providing additional evidence for GB′. Notably, the decay of GB′ during *on* → *off* photoswitching under 505 nm illumination is even faster in more acidic buffers, which indicates that lower pH values may support a more flexible protein local environment with dynamic H-bonding for the light-induced GB′ chromophore.[14,27]

Fs-TA of GA and GA′ in LEA and LEA-A69T upon 400 nm excitation dissects the *off*-to-*on* photoswitching mechanism: primary events

To help resolve the question whether proton transfer occurs in the electronic ground or excited states during the *off* → *on* photoswitching, we compared the fs-TA spectra of GA and GA′ species in LEA upon 400 nm excitation (Fig. 4) along with the key mutant LEA-A69T. We also studied GA in pH 5 buffer (Fig. 4a) where it is the dominant species (Fig. S11, SI). This sample greatly reduces the contribution from FRET (if any) since there is only a minor GB population as a potential FRET acceptor. In contrast, we studied the fs-TA dynamics of the photoswitched *off* state in pH 8 buffer (Fig. 4b) to isolate and excite as much pure GA′ species as possible with minimal GA contributions (*i.e.*, the GA absorption peak is barely visible at pH 8, see Fig. 2a). We also measured and analysed the fs-TA spectra of the LEA and other mutants (both GA and GA′ species) in pH 6–8 buffers (Fig. S12–S15, SI) to provide a more holistic overview of the transient electronic dynamics of neutral green species in LEA.

Overall, fs-TA spectra of neutral chromophores in the LEA and mutants exhibit an excited-state absorption (ESA) band from ~425–470 nm involving GA*/GA′* species (asterisk denotes the excited state S_1; see their weak emission band in Fig. 3a), and a stronger stimulated emission (SE) band near 510 nm due to GB* because its peak position largely matches that of the steady-state emission band (Fig. 3a). The SE feature from GA* is largely hidden by spectral overlap from the ESA that overwhelms this region, consistent with the upward transition oscillator strength of a "dark state" being much larger than that of the downward transition.[45,46] Upon comparing the fs-TA contour plots, we note the most pronounced ESA drop that is accompanied by a concomitant SE increase for GA′* in Fig. 4b, indicative of the highly dynamic nature of GA′ species undergoing an ultrafast photoswitching event. Meanwhile, the GB* SE feature exhibits a delayed rise peaking between 10–100 ps, indicative of an interconversion between two states. Importantly, upon direct excitation of GB in the LEA and mutants with a 490 nm actinic pump, we observed an instantaneous ultrafast rise (<140 fs) within the instrument response function (IRF, see

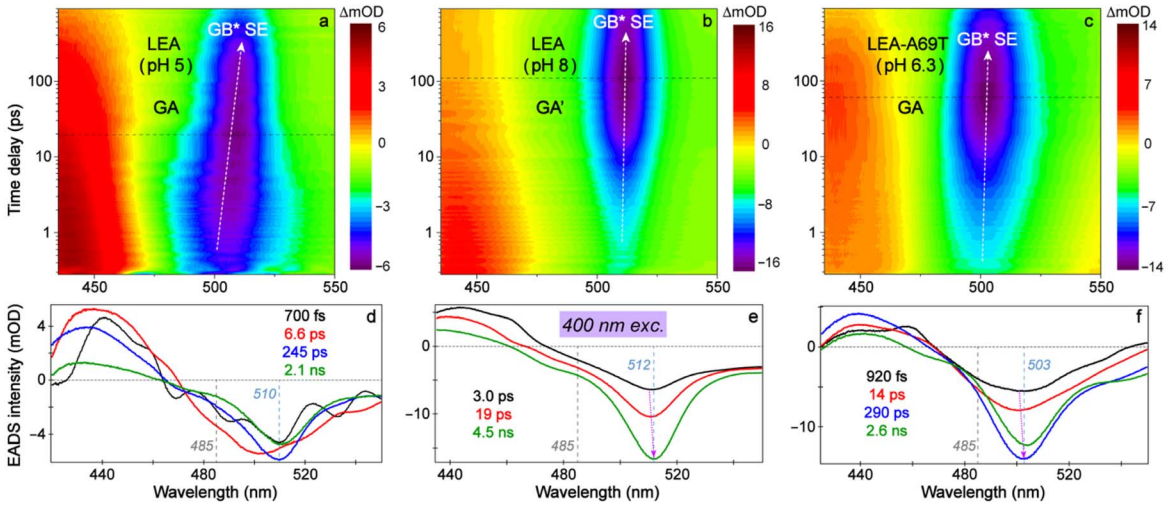

Fig. 4 Transient electronic dynamics of the protonated green species in LEA. Contour plots of fs-TA spectra for (a) GA of the fresh LEA in pH 5 buffer, (b) GA′ of LEA after 505 nm light treatment in pH 8 buffer, and (c) GA of LEA-A69T in pH 6.3 buffer upon 400 nm excitation with global analysis of the corresponding fs-TA spectra shown in panels d–f. In the top panels, the intensity values in milli-optical-density (mOD) units are shown by colour bars, and the vertical time axis is in the logarithmic scale. Dashed arrows highlight the major spectral evolution of the GB* stimulated emission (SE) after GA/GA′ excitation; the horizontal line indicates when the GB* SE reaches its peak maxima. In the bottom panels, evolution-associated difference spectra (EADS) track the sequential evolution (black → red → blue → green) with colour-coded lifetimes. Vertical grey and blue dashed lines highlight the SE shoulder band (~485 nm) and the main SE peak (~510 nm), respectively. The horizontal grey dotted lines represent zero spectral intensity.

the Experimental section below) that is followed by a bi-exponential decay process.[19] The drastically different GB* SE dynamics following 400 *versus* 490 nm excitations suggest that direct excitation of GB does not play a significant role in fs-TA spectra after 400 nm excitation, which allows the tracking of neutral and intermediate species dynamics in S_1.[18,19]

There is a clear difference between the fs-TA spectra upon excitation of GA and GA′ in LEA, which sheds new light on the initial electronic dynamics of *cis*- and *trans*-neutral green species.[15,19] After excitation of the mostly pure *trans* GA′ at pH 8, the GB* SE displays a sustained and substantial intensity increase while the peak position remains largely stagnant (Fig. 4b). The UV/visible (UV/vis) spectra before and after GA′ excitation (Fig. S11, SI) confirm that some *off* → *on* photoswitching occurs during the experiment. In contrast, the mainly *cis*-GA* dynamics in LEA (Fig. 4a) appears more nuanced: there is a clear narrowing of a broad SE band on the fs-to-ps timescale and a pronounced peak redshift throughout the experimental time window.

To better understand the underlying transient processes, we performed global analysis of fs-TA spectra (Fig. 4d–f) with the evolution-associated difference spectra (EADS). The grey vertical line at 485 nm highlights the SE feature (Fig. 4d) where GA* is expected to emit (Fig. 3a).[14] Upon 400 nm excitation of primarily GA in LEA at pH 5, we observe an instantaneous and ultrafast (~140 fs) signal increase in both probe regions where GA* and GB* are expected to emit (Fig. S6, SI), also represented by the black trace (700 fs lifetime; see detailed discussions in the SI on some apparent wavery features due to the initial coherent artifacts) in Fig. 4d. Given the rise within the IRF of the optical setup, direct excitation of some GA and GB species likely contributes to the initially broad SE band; however, the excited-state chromophore dynamics (*e.g.*, ESPT and isomerization) would dictate the subsequent spectral evolution.

In particular, the black trace quickly evolves into the red trace on the 700 fs timescale, tracking Franck–Condon dynamics and initial relaxation of GA* by conformational rearrangement of the chromophore and local environment. In other Kaede-like pcFPs, similar time constants and spectral profiles have been retrieved and attributed to an intermediate species.[30] Notably, the red trace features an SE shoulder at ~485 nm and a primary SE peak at around 500 nm, while the shoulder is only prominent after excitation of the fresh LEA in pH 5 buffer, as highlighted by the normalized EADS (Fig. S15, SI). The GA* SE feature is the most pronounced because any contribution from GB is greatly diminished in this most acidic buffer. The dominant SE peak at ~500 nm may be attributed to I*, which is in between the GA* and GB* SE peaks, likely *via* ESPT en route from the *cis* neutral to *cis* anionic chromophores which continues with a ~10 nm redshift (red → blue trace in Fig. 4d). Given the *cis*-GA species at equilibrium in pH 5 buffer according to its pK_a (~6.3),[11] the pK_a^* (excited-state pK_a) is lowered for FP chromophores and the photoacids in general to promote an ESPT reaction.[22,39,47,48]

The red trace evolves with an ~7 ps lifetime, which involves the fast nonradiative decay of *cis* GA* (~485 nm SE band). The matching GA* decay and GB* SE rise on the 15–20 ps timescale from probe-dependent fits (Fig. S14, SI) supports a two-state model that is consistent with ESPT. Since little photoswitching was observed after GA excitation, there is no clear *cis*-to-*trans* isomerization. The *cis* anionic species (blue and green traces in Fig. 4d) decay with two lifetimes of 245 ps and 2.1 ns,

likely due to inhomogeneous FP chromophore populations with a decent fluorescence quantum yield (FQY) for GB*,[24,49] supported by the matching blue/green traces in normalized EADS (Fig. S15, SI).

Contrastingly, beyond the initial ultrafast signal rise within the IRF, the *trans* GA′ lifetimes *via* global analysis (3 and 19 ps, 4.5 ns in Fig. 4e) largely track the GA′* ESA decay and GB* SE rise, with the latter being more intense than its counterpart after GA excitation (Fig. 4d). The probe-dependent fits at ~485 nm (Fig. S14, SI) reveal that the dominant GB* SE band at around 510 nm may obfuscate the pure GA′* dynamics, since the overlaid peak intensity dynamics in both regions are quite similar. The faster decay of GA′ (3 ps) than GA (6.6 ps) is consistent with the distorted structure of GA′ to promote faster twisting motions and nonradiative decay of the neutral chromophore,[18,33] which likely undergoes the *trans*-to-*cis* isomerization and proceeds through an S_1/S_0 conical intersection before the ultrafast bifurcation to produce *trans* and *cis* neutral species in the hot ground state. Such a model has been invoked for the faster-photoswitching IrisFP,[30] wherein the *cis* neutral species deprotonates in S_0 on much longer timescales (micro-to-milliseconds). Similar isomerization time constants in the FP literature[43,50] agree with the weakly fluorescent nature of GA*. In tandem, the 3 ps time constant also accompanies the GB* SE rise, which could be due to ESPT[22,46,49] or FRET since GB* SE maintains its profile and continues to rise (red → green traces, Fig. 4e) with a 19 ps time constant. Such a FRET pathway may transiently contribute[37,41] in tetrameric FPs like LEA, with inter-chromophore distances governing the FRET efficiencies.[36,38]

Interestingly, X-ray structural comparisons (Fig. 5a) unveil a major factor to rationalize the slow photoswitching in LEA and mEos4b *versus* the much faster photoswitching in IrisFP: the much smaller S173 (than F173) in IrisFP reduces steric hindrance for P-ring twists that are commonly implicated for a photoexcited chromophore.[5,11,16] Meanwhile, structural analysis (Fig. 5b) of the *trans* green *off* state in model pcFPs reveals a Glu144 in the vicinity of the chromophore P-ring end, which lends credence to a potential ESPT pathway.[42,51–53] For comparison, ESPT in wild-type GFP with a water-Ser205-Glu222 H-bonding chain occurs on a ~5 ps timescale.[22] The minor change in the electronic absorption spectra before and after fs-TA measurements (Fig. S11, SI) supports this assignment of ESPT occurrence during photoswitching, which cannot be due to FRET that transfers energy *via* the coupled electric dipoles.[37]

When comparing steady-state absorption and fs-TA spectra of GA *versus* GA′ in LEA-H62X (Fig. S11–S15, SI), the larger increase in GB* SE within ~100 ps upon GA excitation than GA′ excitation does not directly scale to GA/GA′ populations, while the much larger GB population may act as FRET acceptors. Interestingly, the fs-TA spectra of GA′ in LEA and LEA-H62X are very similar (Figs. S12–S15, SI), both in terms of pertinent time constants and transient spectral evolution. This correlation warrants discussions. The *on* → *off* photoswitching in LEA-H62X is much more efficient than that in LEA, resulting in an ~90% reduction of GB absorption and a large GA′ population[18] which should show clear GA′* features but are not supported by global analysis (Fig. S13, SI). This finding points to a rapidly

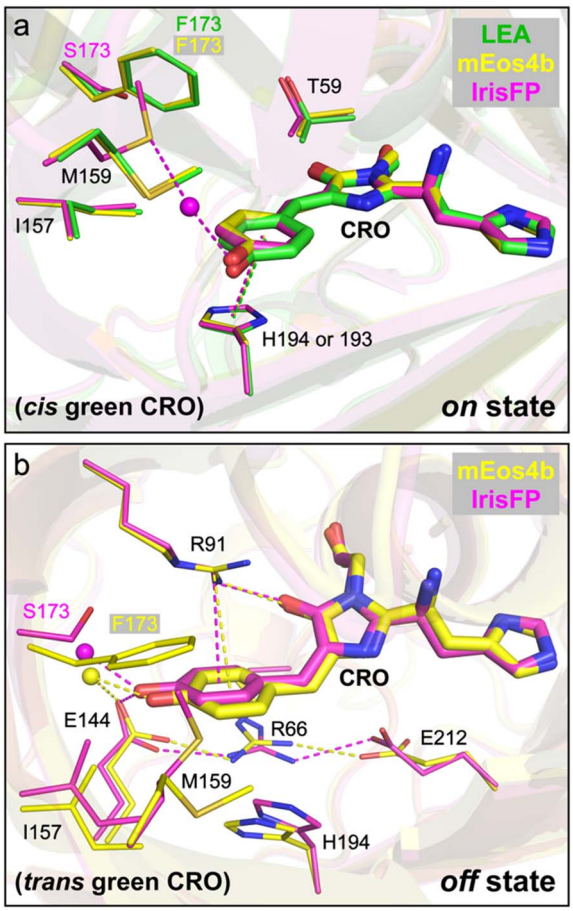

Fig. 5 Overlaid protein pockets of Kaede-like pcFPs in the green *on* and *off* states. (a) Crystal structures of the green *on* state in LEA (green), mEos4b (yellow), and IrisFP (magenta) with PDB IDs of 4DXN,[11] 6GOY,[16] and 2VVH,[5] respectively. (b) Crystal structures of the green *off* state in mEos4b (yellow) and IrisFP (magenta) with PDB IDs of 6GOZ[27] and 2VVI,[5] respectively. The chromophore (CRO) and nearby residues (single-letter abbreviation) are shown by thick and thin sticks, respectively. The oxygen, nitrogen, and sulfur atoms are colored in red, blue, and gold, respectively. Water (if any in the region) is denoted by a sphere in the FP-specific color. The H-bonds, π–π stacking (the chromophore P-ring with an adjacent histidine/H194), and cation-π (the chromophore P-ring with an adjacent arginine/R91) interactions are denoted by dashed lines in the FP-specific colors to highlight differences between FPs.

fleeting GA′ in a distorted state (Figs. 1c and 2b). Different from GA′ in LEA, GA′ in LEA-H62X completely relaxes to the resting state (GB) in the dark,[18] implying a more flexible protein pocket with a reduced barrier for thermal equilibration. The fs-TA spectra of GA and GA′ in LEA-H62X are also similar (Fig. S12, SI). In essence, the GA/GA′ states in LEA-H62X and the GA′ states in LEA have similar ultrafast behaviours after photoexcitation, in correlation with the reduced photoconversion efficiency of GA′ in both LEA and LEA-H62X.[14,18] Given the modification to His62 that is unconjugated in the green chromophore, such dynamic similarities allow us to connect the far-imidazole ring to the P- and I-rings of the chromophore (Fig. 1c). The methyl group on the histidine ring can disrupt surrounding residues in the chromophore pocket through a salt

bridge (H-bonding chain) involving Glu212, Arg66, Glu144, and His194 (Fig. 5b),[17,18,27] which can reduce the LEA photoconversion efficiency (requiring a planar chromophore for the I- and far-imidazole rings)[4,19] but enhance the photoswitching properties (*e.g.*, P-ring twists).[18]

It is notable that His194 is a conserved residue in Kaede-like pcFPs as part of the aforementioned four-residue internal charge network that stabilizes the chromophore to maintain a high FQY, while playing a key role in photoconversion. Two of these residues were assigned apparent pK_a values of ~4.5 (Glu212) and ~7.5 (His194) in LEA that dictate photoconversion efficiency.[11] The protonation state change of His194 from pH 8 → 6 likely influences the spectroscopic properties of both GB and GA′ in *cis* and distorted *trans* conformations, respectively. In the *cis* conformation, His194 maintains π–π stacking interactions with the chromophore phenol/phenolate (P)-ring, which likely contributes to the blueshifted GB absorption as the buffer pH decreases (Fig. 1a). In the distorted *trans* configuration, His194 is further away from the chromophore P-ring based on crystal structures of the *off* state in mEos4b and IrisFP (Fig. 5b).[5,27] Therefore, the protonation state change of His194 likely has an indirect influence on the *trans*-like chromophore through interactions with certain residues in the proximal internal charge network like Glu212, Arg66, and Glu144 (see above). We envision this work to inspire future X-ray crystallography of GA or GA′ species of LEA for a more direct comparison to the depicted *off* state if innovative methods can help isolate these intrinsically "dark" species under physiological pH conditions.[11,32]

Notably, the fs-TA spectra of GA species in LEA-A69T at pH 6.3 (Fig. 4c,f) are quite similar to those of the LEA at pH 6.3 (Fig. S12a, SI), while LEA-A69T does not undergo *on* → *off* photoswitching under 505 nm irradiation. The assignments of EADS and lifetimes of LEA-A69T remain similar to those of LEA, and the second component (14 ps) can have contributions from ESPT and FRET pathways given the much larger rise of the GB* SE peak within ~100 ps as well as a minor kinetic isotope effect of ~1.5 by comparing the GB* SE rise dynamics (Fig. S14e and i, SI). The initial rise of the GB* SE is also larger in LEA-A69T with a more confined chromophore *via* interactions with an adjacent His194 that is π-stacked over the P-ring,[19] likely hindering the P-ring twists and nonradiative decay of GA*. Among all the LEA mutants studied, LEA-A69T displays the most prominent GA* signature due to the elevated chromophore pK_a and more restrictive local environment of LEA-A69T.[17,18] The ~485 nm SE shoulder band tracks GA* (highlighted by overlaid EADS in Fig. S15, SI), which exhibits a ~12 ps time constant from global analysis and probe-dependent fits (Fig. S14, SI), longer than the ~7 ps time constant of GA* in LEA (Fig. 4d). This result is consistent with the more flexible chromophore pocket with Ala69 in LEA particularly near the P-ring.[17,19] Meanwhile, the retrieved longest lifetime of 2.6 ns is smaller than the 4.5 ns lifetime after GA′ excitation (Fig. 4), lending support to the bright GB* formation after 400 nm excitation of the neutral species, mostly efficient for the light-induced GA′ species of LEA. In sum, we can rank the *off* → *on* photoswitching capability of this unique set of comparative FPs in the low-to-high order: GA of LEA < GA of LEA-A69T < GA of LEA-H62X < GA′ of LEA < GA′ of LEA-H62X, which is correlated with green-to-red photoconversion capability in the high-to-low order: GA of LEA > GA of LEA-A69T > GA of LEA-H62X > GA′ of LEA > GA′ of LEA-H62X (Fig. 1d and Fig. S5, SI).[12,14,18,19] As a useful spectral marker, the ~485 nm SE shoulder band is only pronounced in fs-TA for the more photoconvertible GA species, whereas it is much reduced and fleeting with a shorter lifetime for the more photoswitchable GA′ species (Fig. S14 and S15, SI).

FSRS reveals vibrational signatures of the neutral chromophore in LEA-A69T and ultrafast nonradiative decay of *cis*-GA*

The FSRS methodology has emerged as a powerful three-pulse technique using a sequence of fs and ps pulses to track transient molecular structural dynamics of a variety of systems.[23–25,54] It is especially beneficial to study FPs given the broad wavelength tunability of the FSRS setup to target, isolate, and enhance signals from the three-residue chromophore amidst hundreds of amino acids in the protein matrix.[24] We applied ground-state (GS) and excited-state (ES)-FSRS on the much less photoswitchable LEA-A69T to complement prior measurements on the LEA and mutants. Due to the elevated pK_a of LEA-A69T that reduces GB in a pH 6.3 buffer, we used a 400 nm actinic pump to excite fresh GA species along with a ~550 nm Raman pump that provides desirable pre-resonance enhancement with the SE feature.[54,55] In particular, the 552 nm Raman pump beyond the red edge of the GB absorption band (Fig. S11e) avoids enhancement of the *cis*-anionic species, and instead obtains GS-FSRS signatures for dominant GA species of LEA-A69T (Fig. 6b). Though the GS-FSRS peak intensities are much weaker than those collected with a 540 nm Raman pump for LEA-A69T in pH 8 buffer (Fig. S16, SI), key peak frequency shifts within 1200–1300 and 1600–1700 cm^{-1} confirm the P-ring C–O(H) and I-ring C=O/bridge C=C stretching motions of the protonated GA species of LEA-A69T (see illustrations of several Raman marker bands in Fig. S17, SI) in pH 6.3 buffer.[18,24,56] In contrast, the much stronger GB modes at ~1370 and 1540 cm^{-1} dominate GS-FSRS of LEA-A69T in pH 8 buffer (Fig. S16, SI).[57]

The 2D-contour plot of ES-FSRS (Fig. 6a) manifests several prominent transient vibrational peaks that are shifted *versus* their GS-FSRS counterparts (Fig. 6b), which reflect the coupled electronic and vibrational motions of the chromophore going from S_0 to S_1.[22,24] The excited-state peaks are at least twice more intense than many ground-state peaks, mainly due to *cis*-GA species (Fig. S16, SI) which are supported by quantum calculations (see mode assignments in Table S2, SI), although contributions from *cis*-GB still occur due to better resonance conditions with the minor GB population (see Fig. S11, SI). Interestingly, the ~1050 cm^{-1} mode in GS-FSRS of LEA-A69T becomes especially enhanced *versus* other peaks (Fig. 6b), but diminishes after photoexcitation (Fig. 6a). This mode assigned to the CCH bending motions of the chromophore histidine ring (His62; see Fig. S17a, SI) may serve as a sensitive probe to the local environment, and this end of the chromophore does not exhibit rich Franck–Condon dynamics that are associated with

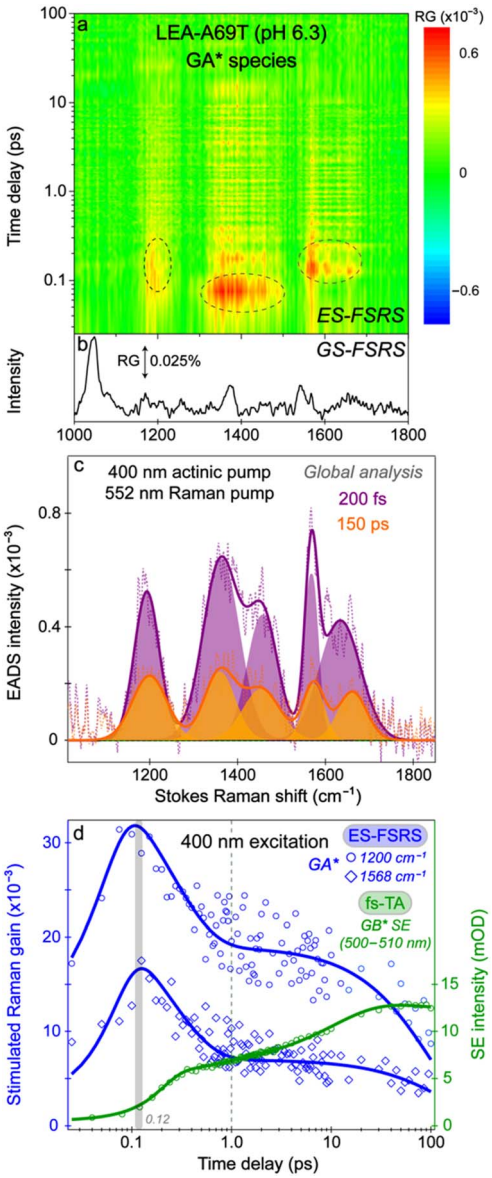

Fig. 6 Transient vibrational signatures of *cis* GA* in LEA-A69T. (a) Contour plots of ES-FSRS of LEA-A69T in pH 6.3 buffer after 400 nm excitation with a 552 nm Raman pump. Intensity values in Raman gain (RG) are shown by using a colour bar, and the vertical time axis is in the logarithmic scale. (b) GS-FSRS of LEA-A69T. The double-sided arrow represents the RG magnitude. (c) Global analysis of the ES-FSRS spectra in panel a. The evolution-associated difference spectra (EADS, dashed lines) represent a sequential scheme with colour-coded lifetimes, overlaid by gaussians from least-squares fits (transparent peaks) and the summation (solid lines). (d) Intensity dynamics from ES-FSRS (blue) and fs-TA (green) of LEA-A69T. Data points (hollow) are overlaid with exponential fits (solid curves). The RG magnitude (blue) is represented by the integrated area of the least-squares-fit gaussians. The probe wavelength region for GB SE is from 500–510 nm. Time delay is in the logarithmic scale. Solid grey and dashed vertical lines denote the peak and plateau of the ES-FSRS peaks.

the conjugated chromophore ring system. In general, the high-frequency peaks (~1580–1700 cm^{-1}) in the ES-FSRS spectra correspond to C=C and C=N stretching motions of P- and I-rings (Fig. S17e and f, SI), while broad peaks from ~1300–1500 cm^{-1} track C–N stretching on the I-ring and C–C stretching and C–H rocking motions on the P-ring (Fig. S17b–d, SI). The ES-FSRS peak centred at ~1200 cm^{-1} is more global involving delocalized H-rocking motions across the P-, I-, and histidine rings.

Notably, the ~1400 cm^{-1} mode peaks slightly earlier than the other modes in the excited state, which we could attribute to the light-induced P → I-ring charge transfer within the Franck–Condon region as an intrinsic property of the FP chromophore,[58] subsequently enabling P-ring twists as an effective energy dissipation pathway after the initial charge migration. This step is well corroborated by the later-peaked ~1200 and 1568 cm^{-1} modes (around 120 fs, Fig. 6) involving P- and far imidazole ring motions (see the 1568 cm^{-1} mode illustration in Fig. S17d, SI), with pertinent twists implicated for the unique photoswitching behaviour of pcFPs such as LEA.[15,19]

Global analysis of ES-FSRS (Fig. 6c) reveals two major lifetimes for transient vibrational peak decay, ~200 fs and 150 ps, due to Franck–Condon relaxation and the average of subsequent radiative and nonradiative processes. The ~150 ps lifetime is much shorter than prior ES-FSRS targeting GB* in the LEA and mutants with an ~2 ns lifetime typical of FPs with bright fluorescent states. Furthermore, ES-FSRS modes monotonically decay after photoexcitation (~250 fs and 100–150 ps from probe-dependent fits), clearly contrasting the biphasic rise of GB* SE intensity (Fig. 6d) with ~600 fs, 10 ps rise and 2.5 ns decay from the probe-dependent fits (Fig. S14, SI). This result reveals that ES-FSRS mainly reflects the GA* decay dynamics instead of the GB* population that is primarily tracked by fs-TA. The strategic tuning of the Raman pump to redder wavelengths than the GB* SE band edge highlights the uniqueness of FSRS to catch fleeting chromophore populations with weak oscillator strengths, achieving the goal of tracking the intrinsic *cis*-GA* dynamics. A direct comparison of ES-FSRS spectra of GA* after 400 nm excitation and GB* after 490 nm excitation near the photoexcitation time zero (Fig. S16c, SI) reinforces this key point. Notably, the relatively fast ~150 ps long time constant involves a much enhanced nonradiative relaxation which is characteristic of a dark or dim (weakly fluorescent) neutral chromophore with reduced interactions to the rather flexible protein local environment.[17,33,59]

Conclusions

With both equilibrium and nonequilibrium spectroscopies, we monitored the formation of the photoswitched *off* state at various buffer pH values and in comparative pcFP scaffolds. Upon near-UV excitation, we compare the photoresponse of native and photoswitched neutral chromophores, which are both photoconvertible, and find that the native *cis* neutral GA form can undergo a rapid nonradiative relaxation to its electronic ground state and also undergo ESPT due to conformational inhomogeneity. In clear contrast, the distorted *trans* GA′ population efficiently returns to the initial nonphotoconvertible *cis* anionic resting state *via* isomerization and proton transfer that underlies the *off* → *on* photoswitching. The benchmarking of ultrafast *cis*-GA* and *trans*-GA′* dynamics in the excited state,

starting from the photoexcitation time zero, provides a holistic portrait of the complex potential energy landscape inside a dynamic protein pocket, which allows for photoswitching of this engineered LEA originally intended only for photoconversion. For GA species in the fresh LEA, LEA-A69T, and LEA-H62X proteins, we can correlate their increased *off* → *on* photoswitching efficiency (in that order) with decreased green-to-red photoconversion after UV excitation.

Based on these mechanistic insights, we propose rational design strategies involving the reduction of potential proton acceptors near the chromophore to inhibit the ESPT reaction (hence avoiding an efficient ultrafast energy dissipation pathway) as well as modification of the intrinsic chromophore properties *via* noncanonical amino acid (ncAA) incorporation[60,61] to achieve an optimal balance between electrostatic and steric effects.[33,59] The His194X could be a target as this π-stacked histidine can affect both the chromophore P-ring flexibility as well as the internal charge network nearby (see Fig. 5 and the associated discussions on the chromophore properties). These strategies may also enhance the photoconversion quantum yield of the photoswitched *off* state, eventually making dual illumination[14,27] involving both 400 and ∼500 nm light a superior illumination condition for rapid photoconversion. This powerful strategy produces more neutral species at physiological pH values or even under basic buffer conditions, increasing the potential reservoir for photoconversion in unique environments. For both the native and photoswitched *off* neutral chromophores, a careful balance between optimizing the chromophore flexibility with planarity and rigidity[33] must be maintained for efficient photoconversion with a high FQY. The engineering of the monomeric LEA (mLEA) would realize substantial progress toward its use in advanced bioimaging techniques,[62,63] in addition to a more sensitive evaluation of the ultrafast dynamics and primary events following near-UV excitation of the neutral chromophore without interference from FRET. Furthermore, we observed some FRET quenching in the LEA on the ∼10 ps timescale, which may diminish photoconversion because the FRET donor and photoconvertible population are one and mixed. On a related note, this work may open the door for ultrafast investigations of FRET pairs, especially involving highly fluorescent FP-based acceptors for sensing applications, which remain understudied throughout the literature.[64,65] We foresee that this work will provide broad informed design principles and inspire vigorous collaborations between ultrafast spectroscopists, protein engineers, and the bioimaging community to enable the next generation of versatile (pc)FPs with targeted properties.

Experimental materials and methods

Protein expression and sample preparation

The Wachter Lab prepared the pcFPs including LEA, LEA-A69T, and ALL-Q62H according to published protocols.[11,17] The Mills Lab prepared the mutant LEA-H62X (X = 3-methyl-histidine) *via* ncAA incorporation with detailed procedures reported in our prior work.[18] Before steady-state, light-emitting diode (LED), and time-resolved spectroscopies, protein samples were placed in a −4 °C fridge to gradually thaw from a −80 °C freezer, and then warmed to room temperature (∼22 °C) in the dark to prevent sample exposure to ambient light. When necessary, FPs were centrifuged to form a precipitate of aggregated or photobleached samples, and the resulting supernatant was pipetted for subsequent measurements or stored in a −4 °C fridge. The samples additionally went through a 0.22 μm filter to reduce light scattering prior to ultrafast experiments. Several buffers with pH values ranging from 5–8 were used to study the LEA and mutants. The pH 8 solution consisted of a 50 mM HEPES-NaOH buffer, and the measured pH was 7.9. The pH 7 solution involved adding HCl to the aforementioned HEPES-NaOH buffer until the measured pH was 6.9–7.0. The pH 6 solution was comprised of 50 mM PIPES buffer with a measured pH of 6.3. The pH 5 solution consisted of a 50 mM citrate buffer with a measured pH of 5.1. All buffer solutions contained 150 mM NaCl and 0.1 mM EDTA.[18] Buffer exchanges were performed with a centrifuge to transfer protein samples using the Centrifugal Filter Units (Millipore) with 2 mL vials (Amicon Ultra) and Centrifugal Filters (Ultracel) involving regenerated cellulose with a 10 KDa molecular weight cutoff.

Steady-state electronic spectroscopy

The steady-state electronic absorption and emission spectra were collected with a JASCO V-760 spectrophotometer and a Shimadzu RF-6000 spectrofluorophotometer, respectively. The samples were housed in a four-sided rectangular quartz cuvette with a 10-mm-pathlength for collecting absorption and emission spectra. For absorption before/after ultrafast measurements, the spectra were collected in a 1-mm-pathlength quartz cuvette (Spectrosil 1-Q-1, Starna Cells, Inc.). Dilute solutions with an optical density (OD) below 0.1 per mm at all wavelengths above ∼250 nm were used for steady-state measurements to reduce self-reabsorption with the 10-mm-pathlength cuvette, except for ultrafast measurements that typically required higher sample concentrations in the 1-mm-pathlength cuvette.[22,24]

Both the photoconversion and photoswitching of the LEA and mutants were observed during fluorescence measurements. We evaluated several parameters including the slit width, scan speed, and sensitivity to maintain sufficient signal quality while limiting phototransformation during spectral measurements. Unless specified otherwise, the scan speed and sensitivity were set to 2000 nm minute^{-1} and low. The slit widths for all the measurements with 360–400 and 490 nm excitations were 5 and 3 nm, respectively. The slit width was reduced upon 490 nm excitation due to signal saturation at the GB emission peak. The cuvettes were placed in the sample compartment immediately before each measurement and removed as soon as the spectral collection ended to reduce any unwanted photoconversion or photoswitching. The absorption spectra were collected before and after each fluorescence measurement to monitor the equilibrium change induced by the excitation source. Due to photoconversion and photoswitching during fluorescence measurements, individual fresh samples were prepared for all fluorescent spectra collected upon excitation of GA to limit

contamination from other chromophore species, including the photoconverted red neutral and anionic species. All steady-state measurements were performed at room temperature.

Photoconversion and photoswitching with a 3D-printed LED box for controlled irradiation

For photoconversion and photoswitching measurements, 400 and 505 nm LEDs (Bivar, Inc.), respectively, were wired into a home-built 3D-printed "dark box" with 16 LEDs total in each, with four LEDs per side. A four-sided rectangular quartz cuvette was placed in the center of the box for an even and controlled illumination. The illumination power of the LEDs was set to ∼9 mW per bulb to be consistent with previous measurements;[14] the illumination power was measured to be ∼2.9 and 1.5 W cm^{-2} for 400 and 505 nm illumination, respectively, at the sample location in the box center. The power was measured using a power meter with a thermal power sensor (S470C, ThorLabs, Inc.). Photoconversion and photoswitching were monitored *via* electronic absorption spectroscopy at predetermined time intervals until the absorption spectra stopped changing, concurrent with the increased photobleaching indicated by an elevated baseline during absorption measurements.

Targeting GB′, the initial photoswitching was performed over 50–80 minutes depending on the buffer pH conditions. The photoswitched samples were placed in a −4 °C fridge overnight, wherein partial thermal recovery of the GA′ and GB/GB′ species occurred. The samples were warmed to room temperature before the subsequent photoswitching measurements, which involved the sequential UV excitation (360–400 nm) triggering *off* → *on* photoswitching during fluorescence measurements, followed by *on* → *off* photoswitching under 505 nm illumination in the LED box. This process was repeated several times, representing the photocycles in Fig. 3c for each excitation (360, 370, 380, 390, and 400 nm). The absorption spectra were collected before and after each fluorescence measurement. All the electronic absorption and emission spectra collected for these sequential experiments involving *on* → *off* and *off* → *on* photoswitching are shown in Fig. S10 in the SI.

Femtosecond transient absorption (fs-TA) and femtosecond stimulated Raman spectroscopy (FSRS)

A thorough description of our homebuilt optical setup for the wavelength-tunable fs-TA and FSRS experiments can be found in prior publications.[48,55,66] The fundamental laser output (∼800 nm center wavelength and 35 fs pulse duration at 1 kHz repetition rate) operates with an average power of ∼3.6 W from a Ti:sapphire regenerative amplifier (Legend Elite-USP-1K-HE, Coherent, Inc.), seeded by a mode-locked Ti:sapphire oscillator (Mantis-5, Coherent, Inc.) all placed on an air-float optical table (RS2000, Newport, Inc.).

The fs-TA measurements with fs, 400 nm excitation involve second harmonic generation (SHG) that doubles the frequency of the 800 nm fundamental pulse before temporal compression *via* a prism pair. A chopper synchronized to half the laser repetition rate (500 Hz) was placed in the actinic pump beampath for signal generation. For FSRS measurements, the same actinic pump was used while the synchronized chopper was placed in the Raman pump beampath. Tunable Raman pump generation involves an fs noncollinear optical parametric amplifier (NOPA), a spectral filter, a second harmonic bandwidth compressor (SHBC), and a two-stage ps NOPA. The Raman pump was tuned to ∼540–550 nm for ground and excited-state FSRS. The probe for fs-TA and FSRS experiments was supercontinuum white light generated by focusing a portion of the fundamental laser output onto a 2-mm-pathlength quartz cuvette filled with deionized water, and then compressed with a chirped mirror pair (DCM-9, 450–950 nm, Laser Quantum, Inc.).

The pump and probe pulses were spatiotemporally overlapped onto a 1-mm-pathlength quartz flow cell with a peristaltic pump to ensure that only fresh sample solution was irradiated throughout the measurements. Due to the photosensitivity of LEA proteins,[11,14] including photoconversion/photoswitching during the 1.5–2 hour data collection, a large sample reservoir (∼5 mL) was constantly flowed to mitigate contamination from the photoinduced species. The UV/visible absorption spectra were collected right before and after each time-resolved measurement to confirm sample stability[22] and monitor any photoconversion or photoswitching that may have occurred. The transmitted probe was focused into an IsoPlane SCT-320 imaging spectrograph (Princeton Instruments, Inc.) before being dispersed onto a PIXIS:100F CCD array camera (Princeton Instruments, Inc.) for signal detection. The 1200 grooves per mm, 500 blaze wavelength and 300 grooves/mm, 300 nm blaze wavelength reflective gratings were utilized for FSRS and fs-TA, respectively. The instrument response function (IRF) with the 400 nm actinic pump was ∼140 fs for all FSRS and fs-TA measurements.[14,55] The actinic pump power was set at ∼0.25 mW for fs-TA, while the Raman pump was set at ∼2.0 mW for the excited-state FSRS to reduce potential dumping of the excited-state population due to resonance with the stimulated emission feature.[18] The pertinent absorption ODs for fs-TA and excited-state FSRS experiments are listed in Table S3 (SI).

Quantum calculations

The gas-phase electronic (ground-state geometric optimization and single-point absorption energy) and vibrational (ground-state Raman) calculations for both the *cis* and *trans* neutral chromophores of LEA were performed using density functional theory (DFT) and/or time-dependent (TD)-DFT at the B3LYP level of theory with 6-311G+(d,p) basis sets. The calculated ground-state Raman spectrum for the *cis* neutral chromophore was scaled to match the experimental FSRS peak frequencies (Fig. 6b) with a scaling factor of 0.985.[67] The representative vibrational normal modes are illustrated in Fig. S17 in the SI. All quantum chemical calculations were performed using the Gaussian 16 software.[68]

Author contributions

Conceptualization: C. F.; methodology and software: T. D. K. and C. C.; formal analysis and investigation: T. D. K. and C. C.;

visualization and validation: T. D. K., C. C. and C. F.; writing – original draft: T. D. K.; writing – review and editing: C. C. and C. F.; supervision and funding acquisition: C. F. All authors have read and agreed to the published version of the manuscript.

Conflicts of interest

There are no conflicts to declare.

Data availability

The datasets with analysis and discussions supporting this article have been incorporated and presented as part of the comprehensive supplementary information (SI). Supplementary information: discussions on steady-state absorption and emission spectra of the contrasting fluorescent proteins (FPs, including the LEA and mutants) in various pH aqueous buffers under light irradiation conditions, quantum calculations of different FP chromophore states *in vacuo*, and comparisons between the chemically and light-induced green neutral chromophore species in aqueous buffer solution with supplementary Fig. S1–S17, Tables S1–S3, and supplementary references. See DOI: https://doi.org/10.1039/d5sc06279a.

Acknowledgements

We are thankful for the financial support from U.S. NSF grant CHE-2433821 and Oregon State University Foundation Patricia Valian Reser Faculty Scholar Endowed Fund in Science to C. F. We are grateful to Profs. Rebekka M. Wachter and Jeremy H. Mills, as well as Dr J. Nathan Henderson at Arizona State University for providing the LEA proteins and mutant samples with helpful discussions.

Notes and references

1 J. S. Biteen, M. A. Thompson, N. K. Tselentis, G. R. Bowman, L. Shapiro and W. E. Moerner, *Nat. Methods*, 2008, **5**, 947–949.
2 K. Nienhaus and G. U. Nienhaus, *Chem. Soc. Rev.*, 2014, **43**, 1088–1106.
3 M. A. Mohr, A. Y. Kobitski, L. R. Sabater, K. Nienhaus, C. J. Obara, J. Lippincott-Schwartz, G. U. Nienhaus and P. Pantazis, *Angew. Chem., Int. Ed.*, 2017, **56**, 11628–11633.
4 R. M. Wachter, J. L. Watkins and H. Kim, *Biochemistry*, 2010, **49**, 7417–7427.
5 V. Adam, M. Lelimousin, S. Boehme, G. Desfonds, K. Nienhaus, M. J. Field, J. Wiedenmann, S. McSweeney, G. U. Nienhaus and D. Bourgeois, *Proc. Natl. Acad. Sci. U. S. A.*, 2008, **105**, 18343–18348.
6 A. Roy, M. J. Field, V. Adam and D. Bourgeois, *J. Am. Chem. Soc.*, 2011, **133**, 18586–18589.
7 J. Wiedenmann, S. Ivanchenko, F. Oswald, F. Schmitt, C. Röcker, A. Salih, K.-D. Spindler and G. U. Nienhaus, *Proc. Natl. Acad. Sci. U. S. A.*, 2004, **101**, 15905–15910.
8 B. Moeyaert, N. Nguyen Bich, E. De Zitter, S. Rocha, K. Clays, H. Mizuno, L. van Meervelt, J. Hofkens and P. Dedecker, *ACS Nano*, 2014, **8**, 1664–1673.
9 N. G. Gurskaya, V. V. Verkhusha, A. S. Shcheglov, D. B. Staroverov, T. V. Chepurnykh, A. F. Fradkov, S. Lukyanov and K. A. Lukyanov, *Nat. Biotechnol.*, 2006, **24**, 461–465.
10 S. F. Field and M. V. Matz, *Mol. Biol. Evol.*, 2010, **27**, 225–233.
11 H. Kim, T. J. Grunkemeyer, C. Modi, L. Chen, R. Fromme, M. V. Matz and R. M. Wachter, *Biochemistry*, 2013, **52**, 8048–8059.
12 B. Breen, J. P. Whitelegge and R. M. Wachter, *Protein Sci.*, 2024, **33**, e5069.
13 K. Nienhaus and G. U. Nienhaus, *ACS Nano*, 2016, **10**, 9104–9108.
14 T. D. Krueger, L. Tang, L. Zhu, I. L. Breen, R. M. Wachter and C. Fang, *Angew. Chem., Int. Ed.*, 2020, **59**, 1644–1652.
15 A. Maity, J. Wulffelé, I. Ayala, A. Favier, V. Adam, D. Bourgeois and B. Brutscher, *Adv. Sci.*, 2024, **11**, 2306272.
16 E. De Zitter, D. Thédié, V. Mönkemöller, S. Hugelier, J. Beaudouin, V. Adam, M. Byrdin, L. Van Meervelt, P. Dedecker and D. Bourgeois, *Nat. Methods*, 2019, **16**, 707–710.
17 H. Kim, T. Zou, C. Modi, K. Dörner, T. J. Grunkemeyer, L. Chen, R. Fromme, M. V. Matz, S. B. Ozkan and R. M. Wachter, *Structure*, 2015, **23**, 34–43.
18 T. D. Krueger, J. N. Henderson, I. L. Breen, L. Zhu, R. M. Wachter, J. H. Mills and C. Fang, *Front. Chem.*, 2023, **11**, 1328081.
19 T. D. Krueger, L. Tang, C. Chen, L. Zhu, I. L. Breen, R. M. Wachter and C. Fang, *Protein Sci.*, 2023, **32**, e4517.
20 R. M. Wachter, *Int. J. Mol. Sci.*, 2017, **18**, 1792.
21 L. Tang and C. Fang, *Int. J. Mol. Sci.*, 2022, **23**, 6459.
22 C. Fang, R. R. Frontiera, R. Tran and R. A. Mathies, *Nature*, 2009, **462**, 200–204.
23 D. R. Dietze and R. A. Mathies, *ChemPhysChem*, 2016, **17**, 1224–1251.
24 C. Fang and L. Tang, *Annu. Rev. Phys. Chem.*, 2020, **71**, 239–265.
25 G. Batignani, C. Ferrante, G. Fumero, M. Martinati and T. Scopigno, *Nat. Rev. Methods Primers*, 2024, **4**, 34.
26 C. Duan, V. Adam, M. Byrdin, J. Ridard, S. Kieffer-Jaquinod, C. Morlot, D. Arcizet, I. Demachy and D. Bourgeois, *J. Am. Chem. Soc.*, 2013, **135**, 15841–15850.
27 E. De Zitter, J. Ridard, D. Thédié, V. Adam, B. Lévy, M. Byrdin, G. Gotthard, L. Van Meervelt, P. Dedecker, I. Demachy and D. Bourgeois, *J. Am. Chem. Soc.*, 2020, **142**, 10978–10988.
28 J. Wulffelé, A. Maity, I. Ayala, S. Gambarelli, B. Brutscher and D. Bourgeois, *J. Am. Chem. Soc.*, 2025, **147**, 10357–10368.
29 A. Fatima, Y. He, J. N. Iuliano, G. M. Greetham, P. Malakar, C. R. Hall, H. A. Woroniecka, B. C. Richardson, J. B. French, A. Lukacs, P. Tonge and S. R. Meech, *Chem. Sci.*, 2025, **16**, 16955–16969.
30 J.-P. Colletier, M. Sliwa, F.-X. Gallat, M. Sugahara, V. Guillon, G. Schirò, N. Coquelle, J. Woodhouse, L. Roux, G. Gotthard, A. Royant, L. M. Uriarte, C. Ruckebusch, Y. Joti, M. Byrdin,

E. Mizohata, E. Nango, T. Tanaka, K. Tono, M. Yabashi, V. Adam, M. Cammarata, I. Schlichting, D. Bourgeois and M. Weik, *J. Phys. Chem. Lett.*, 2016, **7**, 882–887.
31 J. Chang, M. G. Romei and S. G. Boxer, *J. Am. Chem. Soc.*, 2019, **141**, 15504–15508.
32 A. Fadini, C. D. M. Hutchison, D. Morozov, J. Chang, K. Maghlaoui, S. Perrett, F. Luo, J. C. X. Kho, M. G. Romei, R. M. L. Morgan, C. M. Orr, V. Cordon-Preciado, T. Fujiwara, N. Nuemket, T. Tosha, R. Tanaka, S. Owada, K. Tono, S. Iwata, S. G. Boxer, G. Groenhof, E. Nango and J. J. van Thor, *J. Am. Chem. Soc.*, 2023, **145**, 15796–15808.
33 C. Chen, V. Pathiranage, W. S. Y. Ong, S. C. Dodani, A. R. Walker and C. Fang, *Proc. Natl. Acad. Sci. U. S. A.*, 2025, **122**, e2508094122.
34 N. S. Makarov, C. Cirloganu, J. W. Perry, K. A. Lukyanov and K. M. Solntsev, *J. Photochem. Photobiol. A Chem.*, 2014, **280**, 5–13.
35 M. Chattoraj, B. A. King, G. U. Bublitz and S. G. Boxer, *Proc. Natl. Acad. Sci. U. S. A.*, 1996, **93**, 8362–8367.
36 E. A. Jares-Erijman and T. M. Jovin, *Nat. Biotechnol.*, 2003, **21**, 1387–1395.
37 D. W. Piston and G.-J. Kremers, *Trends Biochem. Sci.*, 2007, **32**, 407–414.
38 L. Tang, R. M. Bednar, N. D. Rozanov, M. L. Hemshorn, R. A. Mehl and C. Fang, *Nat. Sci.*, 2022, **2**, e20220028.
39 P. Zhou and K. Han, *Acc. Chem. Res.*, 2018, **51**, 1681–1690.
40 H. Hosoi, H. Mizuno, A. Miyawaki and T. Tahara, *J. Phys. Chem. B*, 2006, **110**, 22853–22860.
41 E. Fron, M. Sliwa, V. Adam, J. Michiels, S. Rocha, P. Dedecker, J. Hofkens and H. Mizuno, *Photochem. Photobiol. Sci.*, 2014, **13**, 867–874.
42 T. D. Krueger, C. Chen and C. Fang, *Chem.–Asian J.*, 2023, **18**, e202300668.
43 S. P. Laptenok, A. A. Gil, C. R. Hall, A. Lukacs, J. N. Iuliano, G. A. Jones, G. M. Greetham, P. Donaldson, A. Miyawaki, P. J. Tonge and S. R. Meech, *Nat. Chem.*, 2018, **10**, 845–852.
44 D. Bourgeois and V. Adam, *IUBMB Life*, 2012, **64**, 482–491.
45 R. Berera, R. van Grondelle and J. M. Kennis, *Photosynth. Res.*, 2009, **101**, 105–118.
46 T. D. Krueger, L. Tang and C. Fang, *Biosensors*, 2023, **13**, 218.
47 R. Simkovitch, S. Shomer, R. Gepshtein and D. Huppert, *J. Phys. Chem. B*, 2015, **119**, 2253–2262.
48 W. Liu, Y. Wang, L. Tang, B. G. Oscar, L. Zhu and C. Fang, *Chem. Sci.*, 2016, **7**, 5484–5494.
49 S. R. Meech, *Chem. Soc. Rev.*, 2009, **38**, 2922–2934.
50 E. Fron, C. Flors, G. Schweitzer, S. Habuchi, H. Mizuno, R. Ando, F. C. De Schryver, A. Miyawaki and J. Hofkens, *J. Am. Chem. Soc.*, 2007, **129**, 4870–4871.
51 K. D. Piatkevich, V. N. Malashkevich, S. C. Almo and V. V. Verkhusha, *J. Am. Chem. Soc.*, 2010, **132**, 10762–10770.
52 C. Randino, M. Moreno, R. Gelabert and J. M. Lluch, *J. Phys. Chem. B*, 2012, **116**, 14302–14310.
53 L. M. Oltrogge and S. G. Boxer, *ACS Cent. Sci.*, 2015, **1**, 148–156.
54 C. Fang, L. Tang, B. G. Oscar and C. Chen, *J. Phys. Chem. Lett.*, 2018, **9**, 3253–3263.
55 L. Tang, L. Zhu, M. A. Taylor, Y. Wang, S. J. Remington and C. Fang, *Molecules*, 2018, **23**, 2226.
56 L. Tang, W. Liu, Y. Wang, L. Zhu, F. Han and C. Fang, *J. Phys. Chem. Lett.*, 2016, **7**, 1225–1230.
57 C. Chen, J. N. Henderson, D. A. Ruchkin, J. M. Kirsh, M. S. Baranov, A. M. Bogdanov, J. H. Mills, S. G. Boxer and C. Fang, *Int. J. Mol. Sci.*, 2023, **24**, 11991.
58 P. Altoè, F. Bernardi, M. Garavelli, G. Orlandi and F. Negri, *J. Am. Chem. Soc.*, 2005, **127**, 3952–3963.
59 M. G. Romei, C.-Y. Lin, I. I. Mathews and S. G. Boxer, *Science*, 2020, **367**, 76–79.
60 J. C. Peeler and R. A. Mehl, Site-specific incorporation of unnatural amino acids as probes for protein conformational changes, in *Unnatural Amino Acids: Methods and Protocols*, ed. L. Pollegioni and S. Servi, Humana Press, New York, NY, 2012, Ch. 8, pp. 125–134.
61 C. Chen, H. Zhang, J. Zhang, H. Ai and C. Fang, *Phys. Chem. Chem. Phys.*, 2023, **25**, 15624–15634.
62 K. D. Piatkevich, J. Hulit, O. M. Subach, B. Wu, A. Abdulla, J. E. Segall and V. V. Verkhusha, *Proc. Natl. Acad. Sci. U. S. A.*, 2010, **107**, 5369–5374.
63 H.-w. Ai, M. A. Baird, Y. Shen, M. W. Davidson and R. E. Campbell, *Nat. Protocols*, 2014, **9**, 910–928.
64 G.-J. Kremers, J. Goedhart, E. B. van Munster and T. W. J. Gadella, *Biochemistry*, 2006, **45**, 6570–6580.
65 P. Trigo-Mourino, T. Thestrup, O. Griesbeck, C. Griesinger and S. Becker, *Sci. Adv.*, 2019, **5**, eaaw4988.
66 L. Zhu, W. Liu and C. Fang, *Appl. Phys. Lett.*, 2014, **105**, 041106.
67 J. P. Merrick, D. Moran and L. Radom, *J. Phys. Chem. A*, 2007, **111**, 11683–11700.
68 M. J. Frisch, G. W. Trucks, H. B. Schlegel, G. E. Scuseria, M. A. Robb, J. R. Cheeseman, G. Scalmani, V. Barone, G. A. Petersson, H. Nakatsuji, X. Li, M. Caricato, A. V. Marenich, J. Bloino, B. G. Janesko, R. Gomperts, B. Mennucci, H. P. Hratchian, J. V. Ortiz, A. F. Izmaylov, J. L. Sonnenberg, D. Williams-Young, F. Ding, F. Lipparini, F. Egidi, J. Goings, B. Peng, A. Petrone, T. Henderson, D. Ranasinghe, V. G. Zakrzewski, J. Gao, N. Rega, G. Zheng, W. Liang, M. Hada, M. Ehara, K. Toyota, R. Fukuda, J. Hasegawa, M. Ishida, T. Nakajima, Y. Honda, O. Kitao, H. Nakai, T. Vreven, K. Throssell, J. A. Montgomery, J. E. Peralta, F. Ogliaro, M. J. Bearpark, J. J. Heyd, E. N. Brothers, K. N. Kudin, V. N. Staroverov, T. A. Keith, R. Kobayashi, J. Normand, K. Raghavachari, A. P. Rendell, J. C. Burant, S. S. Iyengar, J. Tomasi, M. Cossi, J. M. Millam, M. Klene, C. Adamo, R. Cammi, J. W. Ochterski, R. L. Martin, K. Morokuma, O. Farkas, J. B. Foresman and D. J. Fox, *Gaussian 16, Revision C.01*, Gaussian, Inc., Wallingford, CT, 2016.